Multi-Component Heart Reconstruction from Volumetric Imaging

Chandrajit Bajaj *
Department of Computer Sciences,
Computational Visualization Center,
Institute of Computational Engineering and Sciences,
University of Texas at Austin,
Austin, TX 78712

Samrat Goswami †
Department of Computer Sciences,
Computational Visualization Center,
Institute of Computational Engineering and Sciences,
University of Texas at Austin,
Austin, TX 78712

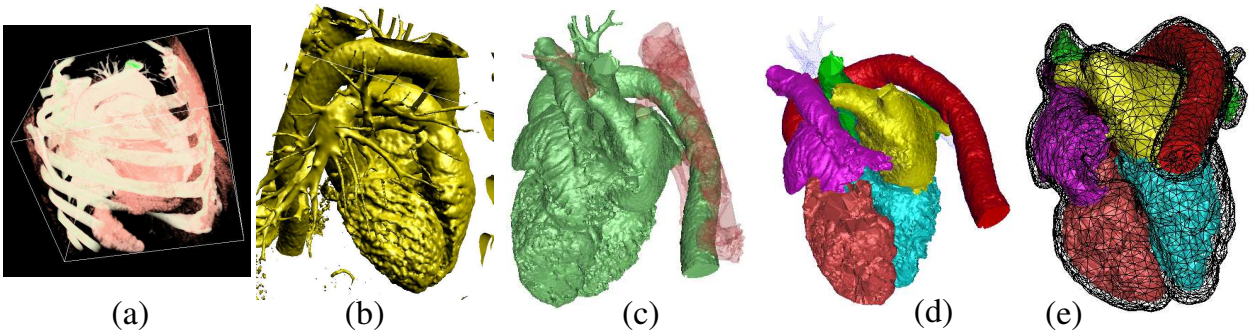

Figure 1: *Snapshots of the data passing through the* IMAGING-TO-MODELING *software system for modeling patient-specific human heart from CT Angio imaging data. (a) Volume rendering of the input imaging data. (b) Initial geometric model extracted from the data. (c) Spurious, noisy parts (transparent red) from the initial model are detected and removed to obtain a clean heart geometry (green) (Section 3.1). (d) The geometry is further segmented and annotated according to the six main compartments of heart (Section 3.2). (e) The muscle wall of the patient heart is built by computing anatomically correct offset surface from (d) (Section 4).*

Abstract

Computer Tomography (CT) and in particular super fast, 64 and 256 detector CT has rapidly advanced over recent years, such that high resolution cardiac imaging has become a reality. In this paper, we briefly introduce a framework that we have built to construct three dimensional (3D) finite-element and boundary element mesh models of the human heart directly from high resolution CT imaging data. Although, the overall IMAGING-MODELING framework consists of image processing, geometry processing and meshing algorithms, our main focus in this paper will revolve around three key geometry processing steps which are parts of the so-called IMAGING-MODELING framework. These three steps are geometry cleanup or CURATION, anatomy guided annotation or SEGMENTATION and construction of GENERALIZED OFFSET SURFACE. These three algorithms, due to the very nature of the computation involved, can also be thought as parts of a more generalized modeling technique, namely geometric modeling with *distance function*. As part of the results presented in the paper, we will show that our algorithms are robust enough to effectively deal with the challenges posed by the real-world patient CT data collected from our radiologist collaborators.

CR Categories: F.2.2 [Nonnumerical Algorithms and Problems]: Geometrical problems and computations; I.3.5 [Computational Geometry and Object Modeling]: Curve, surface, solid and object representations

Keywords: CT-Angio Imaging, Distance Function, Voronoi diagram, Delaunay triangulation, Stable Manifold.

*e-mail:bajaj@cs.utexas.edu
†e-mail:tarmas@gmail.com

1 Introduction

Computer aided diagnosis and treatment of cardiovascular disease, in particular atherosclerosis, left ventricular hypertrophy, valvular dysfunction, increasingly rely on faithful patient specific mesh models of heart that can be used in full-cycle simulation of pulsatile blood flow through the heart. An emerging methodology to construct spatially realistic human heart models is via super fast, 64 and 256 detector (high resolution) Computer Tomographic (CT) imaging [Toshiba Medical Systems - 64 Slice CT 2006]. To further emphasize the premise of modeling heart from patient-specific imaging data, we state a few computational biomedical modeling and simulation examples: 3D computational modeling of the human heart for a quantitative analysis of cyclical electrical conductance on the heart membrane [Luo and Rudy 1991; Luo and Rudy 1994; Hodgkin and Huxley 1952; Hille 1992; Winslow et al. 2000]; the biomechanical properties (stress-strain, elasticity) of the heart ventricular walls [Vetter et al. 1998; Rogers and McCulloch 1994; Rudy and Plonsey 1980; Costa et al. 1996; Hunter et al. 1988; Sachse 2004]; and 3D modeling and simulation of pulsatile blood flow through human arteries/veins for vascular by-pass surgery preplanning on a patient specific basis [Taylor et al. 1998b; Taylor et al. 1998a; Taylor et al. 1999; Sahni 2005; Sahni et al. 2005; Yin et al. 2005]. A finite element decomposition of the geometric domain, capturing the detailed spatial features that can be gleaned from the imaging, is therefore the essential first step toward performing the

necessary numerical simulations [Hackbusch 1985; Braess 1995; Brown et al. 1989; de Munck 1992].

Because of such paramount medical importance, modelers have tried to capture the geometry and displacements from static and dynamic imaging. While some prior papers have attempted to geometrically model the entire human heart [Mari et al. 2001; Veistera and Lotjonen 2001; Allouche et al. 2001], others have mainly focused on functional modeling of cardiac tissue to estimate and study electrical and mechanical properties of the myocardium or ventricular walls [Simelius et al. 2001; Tilg et al. 2001; Muller et al. 2001; McVeigh et al. 2001]. However, very few papers provide a comprehensive computational processing pipeline for modeling the human heart based on patient-specific imaging data[Bajaj et al. 2006]. In this paper, we describe a unified 3D reconstruction and geometric modeling framework that integrates various image processing and geometry processing functionalities that are needed to accomplish this task. A more detailed description of the so-called IMAGING-TO-MODELING framework for modeling patient-specific cardiovascular anatomy being out of the scope of this paper, we focus primarily on three algorithmic components of the geometry processing stage. These three components are CURATION or geometry cleanup, SEGMENTATION of the inner wall into anatomically relevant sub-components, and GENERALIZED OFFSETING to construct the outer wall of the heart from the annotated multi-component inner wall.

The organization of the paper is as follows. In Section 2.1 we give a brief description of the framework including the kind of input data being processed, so that the reader can appreciate the context of the algorithms that we further describe in the subsequent sections. In Section 2.2 we give a brief information on the necessary theoretical and computational background, mainly dealing with distance function. Due to fundamental similarity of the algorithm applied for curation and segmentation, we discuss them together in Section 3. In Section 4 we describe the construction of anatomically correct outer wall from the segmented inner wall of patient heart using generalized offset technique. Finally, we show the performance of these techniques on a real-world imaging data in Section 5 and conclude in Section 6 with insights and future directions of research.

2 IMAGING-TO-MODELING Framework

2.1 Background

Computer aided diagnosis and treatment relies on the creation of a suitably discretized and spatially realistic geometric model from CT imaging data. In this Section, we describe a complete software system that takes the input imaging data from the scanners and builds a linear and/or higher order meshed model of the inner and outer wall of the patient heart. Although the description of all the components of this software system is outside the scope of this paper, we, nevertheless, indulge ourselves to a brief description to put the rest of the paper in proper context.

The imaging data that we obtain as the output of CT-Scan essentially gives a three dimensional description of the patient heart and the surrounding tissue and bone structure. In particular, a dye is injected into the blood-stream of the patient, and as it circulates the patient heart, images of the heart and its surroundings are taken using a scanner. This scanning process is often challenged by several factors, like motion blur (as the heart is breathing), differing contrast of the dye in different chambers of the heart (as the contrast of the dye decreases as time passes) and its limited ability to distinguish between materials (tissue and bone) of nearly same density. These topics are currently under investigation by the radiologists and we point the interested readers to any standard source of publication in this area for a detailed description of the ability, use and shortcomings of one such state-of-the-art instrument [Goerres et al. 2002; Pinsky et al. 2006]. Moreover, since the dye passes through the blood-stream, using CT scanner, one can only obtain information of the inner-wall of the heart where the blood contacts. The chambers of the heart surrounded by the inner wall is therefore often called the *blood volume*.

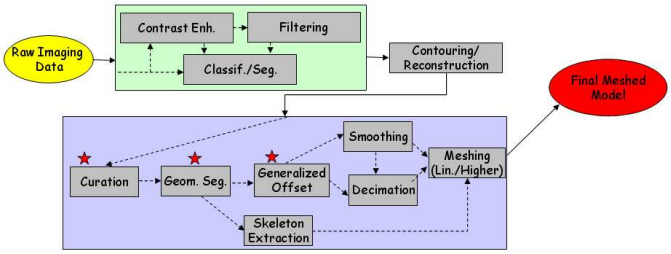

Figure 2: *Data Flow for Modeling Patient-Specific Human Heart. The steps marked with asterix are discussed in this paper.*

As modeleres of a biological system, although we are limited by the performance of the scanning instrument, we would like to do our best to bring out the essential features using the computational tools that we have in our possession. Toward that goal, we have built a comprehensive system which takes an imaging data, possibly flawed with insufficient contrast and noise, and applies a series of image processing algorithms to improve the quality of the input. It then applies the geometry processing algorithms to clean-up the initially extracted geometry and segments the inner-wall into anatomically accurate sub-parts, namely left and right `ventricle`, left and right `atrium`, `aorta`, and `pulmonary artery`, and finally builds a geometric model of the outer wall from this annotated atlas. As mentioned earlier, we will describe the algorithmic foundations of these three steps in the subsequent subsections. Finally, we build a linear (triangle/tet) or higher-order (A-patch, NURBS, quad/hex) mesh of the inner wall, outer wall and the volume in-between to complete the process. Figure 2 shows a schematic diagram of the whole framework with all the modules encapsulated and the data flow between them. The dashed arrows imply that a DAG (directed acyclic graph) of the modules inside every unit is a possible scheduling of the operations and a certain assignment is usually chosen by the user depending on the nature and quality of the imaging data.

The overall framework is built with two main processing units - Image Processing and Geometry Processing. The image processing unit has the modules for contrast enhancement [Yu and Bajaj 2004], denoising [Bajaj and Xu 2003], image segmentation [Yu and Bajaj 2002] and contouring/reconstruction [Lorensen and Cline 1987; Dey and Goswami 2003; Dey and Goswami 2004]. The geometry processing unit consists of curation and geometry segmentation (Section 3), skeleton extraction [Goswami et al. 2006], muscle wall construction (Section 4), denoising [Bajaj and Xu 2003] and decimation [Bajaj and Xu 2001]. The mesh generation unit is also part of geometry processing and it has its own modules for linear and higher order surface and volumetric mesh generation [Bajaj and Xu 2001; Goswami et al. 2007; Labelle and Shewchuk 2007; Zhang et al. 2008]. While the rest of the algorithms are known and can be found in the corresponding papers cited therewith, here we focus on the steps of curation, geometry segmentation and muscle wall construction.

The snapshot of the raw input data passing through the different

stages of our software system is shown in Figure 1. Subfigure (a) shows the volume rendering of a CT64 dataset. The rest of figure shows the initial geometry extracted from the processed imaging data (cluttered with bones and other tissues), curated geometry (after removing all the unnecessary parts), annotated atlas of the inner wall (colored according to anatomical sub-parts), and the wireframe rendering of the suitably inflated outer wall with the segmented inner wall inside.

2.2 Definitions and Notations

In this subsection, we briefly review some of the basic concepts related to distance function and its critical points. Readers must note that an in-depth dealing of these concepts can be found in the papers cited in this subsection, e.g. [Dey et al. 2003; Goswami et al. 2006].

Distance Function and Its Critical Points: Given a compact surface Σ, a distance function h_Σ assigns to every point $x \in \mathbb{R}^3$, the distance to its closest point in Σ. When Σ is sampled by a finite set of points P, h_Σ can be approximated with h_P which assigns to every $x \in \mathbb{R}^3$, the distance to the closest sample point in P. Distance function h_Σ and its approximation has been used earlier for geometric modeling. The distance function has been traditionally used for sample based geometric modeling, *e.g.* reconstruction [Edelsbrunner 2002; Giesen and John 2003], medial axis approximation [Chazal and Lieutier 2004], and feature analysis [Dey et al. 2003; Goswami et al. 2006]. However, very few past works have tried to establish connection between the distance function induced by a shape with its biological characteristics [Edelsbrunner et al. 1998]. Recently, Bajaj and Goswami have demonstrated a novel use of distance function at molecular scale [Bajaj and Goswami 2006]. In this paper, we provide evidences that, even at a much higher scale (organ level), distance function based modeling techniques prove to be extremely useful in bringing out essential features of human anatomy which are then used to build patient-specific models of the same.

The critical points of h_P is intimately related with the Voronoi/Delaunay diagram of P. In particular, Siersma showed that the critical points can be detected by checking the intersection of the Voronoi elements with their dual Delaunay simplices [Siersma 1999]. This leads to the nice connection that we use in this paper - *maxima* are the Voronoi vertices which lie inside their dual Delaunay tetrahedra; the *minima* are the sample points themselves as they lie inside their Voronoi cells, the *index 2* saddle points are the intersections of the Delaunay triangles with dual Voronoi edges, and *index 1* saddle points are the intersections of the Voronoi faces with their dual Delaunay edges. Note that index of a saddle point indicates the number of independent directions the function decreases locally around the critical point. Below we mention some of the basic facts about the distance function (h_P) values at the critical points.

Fact 1 *Let c be a critical point that belongs to a Delaunay simplex σ, then $h_P(c)$ equals the radius of the smallest ball enclosing σ.*

Note, when c is a maximum, $h_P(c)$ is the circumradius of the corresponding Delaunay tetrahedron, when c is an index-2 saddle, $h_P(c)$ is the circumradius of the Delaunay triangle, and so on.

If a point $x \in \mathbb{R}^3$ is allowed to move in the direction of the gradient of h_P, it traces a path in $\mathbb{R}^3$, and eventually ends at a critical point, say c. All such points which end at c this way, forms the set which is defined as the *stable manifold* of c. The computation of the stable manifolds of the critical points is described in the next Section as this is the main ingredient for curation and segmentation. Without going into generalization, we state another fact,

Fact 2 *Let c_1 and c_2 be two maxima whose stable manifolds share a common boundary made by the stable manifold of an index-2 saddle s, then $min\{h_P(c_1), h_P(c_2)\} \geq h_P(s)$.*

3 Curation and Segmentation

After the image processing operations on the raw imaging data are performed, an initial geometric model is extracted. There are primarily two ways to extract one such model. Either one can perform isocontouring (e.g. Marching Cubes [Lorensen and Cline 1987] or Dual Contouring [Ju et al. 2002]), or one can treat the centers of the boundary voxels of a region resulting from image segmentation as scattered points, and perform a point-cloud based reconstruction [Dey and Goswami 2003; Dey and Goswami 2004]. In this paper, the results that we show start with the geometry extracted via contouring using Marching Cubes method. In any case, for the abstraction of the curation problem, we assume that we have a triangulated surface model Σ and a set of points P sampling Σ. Visualization of one such geometric model can be seen in Figure 3(a).

This model is not suitable for many reasons. First of all, it is not often a closed surface, especially when the chosen isovalue is such that the contour crosses the bounding box of the imaging data (Figure 3(c)). Secondly, as Figure 3(b) shows, it has many spurious components, like thin blood vessels, surrounding bones etc. which are not only excess for the modeling of patient heart, but negatively impact further processing and simulations as the model gets unnecessarily large and detailed. Finally, the left and right sub-parts of the inner walls of the human heart should be ideally separated from each other as there is a muscle wall between them. But in the initial model they are often connected by thin bridges (Figure 3 (d)). Therefore, we need a user-guided geometry clean-up of the initial model. However the initial geometry is so complex that any computational tool that aides the user-intervention in a meaningful way is indispensable. We use the critical points of the distance function h_P induced by P to build such a computational tool.

Our algorithm computes the stable manifolds of the maxima of h_P following the algorithm given in [Dey et al. 2003]. We briefly mention this algorithm just for the completeness of this paper.

Stable Manifold Computation: The stable manifolds of the critical points of h_P can be computed from the Voronoi and Delaunay diagram of P. Giesen and John first described the computation of stable manifold of the critical points of h_P in [Giesen and John 2003]. However since stable manifolds may not be sub-complex of Del$P$, approximating them with Delaunay simplices was necessary and was done in [Dey et al. 2003].

Let two Delaunay tetrahedra be σ and σ' which share a common triangle t. We say $\sigma < \sigma'$, if the circumcenter of σ lies in the half-space defined by t that does not contain the fourth vertex of σ. Note, by the property of Delaunay triangulation, the relation $<$ is asymmetric, *i.e.*$\sigma < \sigma' \Rightarrow \sigma' \not< \sigma$. In $\mathbb{R}^3$, however σ' is not always unique for σ. Still, this can be shown that, σ can have at most two neighbors σ_1 and σ_2, for which $\sigma < \sigma_1$ and $\sigma < \sigma_2$. Also, it is to be noted, that the Delaunay tetrahedron σ_{max} whose dual Voronoi vertex is a maximum, has none of its neighbors σ' for which $\sigma_{max} < \sigma'$. The maxima are first sorted in descending order according to h_P. Then the algorithm proceeds with each tetrahedron containing a maximum and collects all the tetrahedra following the

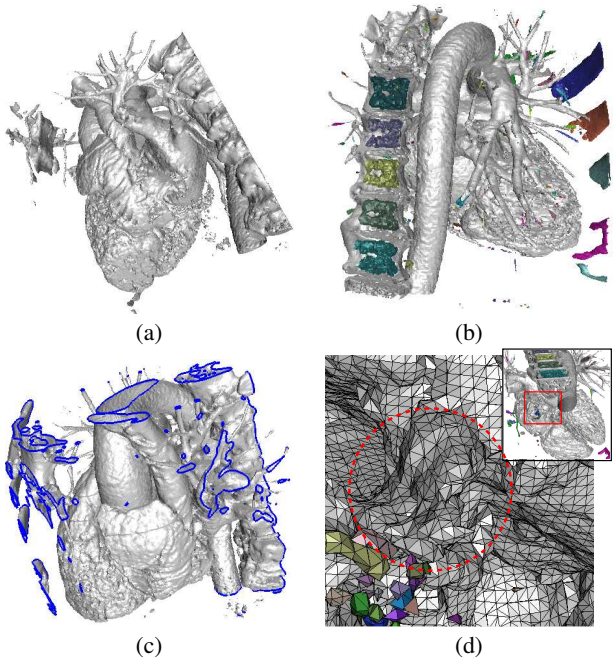

Figure 3: *(a) An initial model of patient heart extracted from the imaging data using Marching Cubes. (b) The model has more than one component. The component containing heart is shown in white while the rest of them are colored. (c) The initial model is not a closed surface. The edges surrounding the cracks are drawn in blue. Note the blood vessels and some of the bones and tissues are connected with the heart. (d) Close-up of the connecting thin bridge between the left and right sub-parts marked by red circle.*

relation $<$. This forms a partition of all the tetrahedra into the stable manifolds of the maxima of h_P.

3.1 Curation

We pose the problem of curation as follows: Given a triangulated input surface Σ, possibly with more than one connected component, how can one identify the noisy and irrelevant features and remove them?

Clearly, it is subjective as to what one calls spurious or noisy features and moreover it heavily depends on the application. For our purpose, we notice that in the initial model, the patient heart is the most voluminous part and either that is disjoint from the surrounding tissues and bones, or the connection between the heart and the surrounding components are very thin. To further quantify this observation, we recourse to the stable manifolds of the maxima of h_P. Before we proceed to the curation algorithm, we want to mention an important prior step, that is marking every maximum as `in` or `out`.

In-Out Marking of Maxima: Since Σ may not be closed (Figure 3(c)), it is not possible to unambiguously tag any point in $\mathbb{R}^3 \setminus \Sigma$ as `in` or `out` w.r.t. Σ. However, based on the imaging data, one can orient the normal vector at any point on the isocontour so that it points outward. Now, even if Σ is not closed, it still locally carries the notion of `in` and `out` which is all we need to tag a maximum as `in` or `out`.

A maximum is a Voronoi vertex c which lies inside its dual Delaunay tetrahedron $\sigma = \text{convex hull}(v_1, v_2, v_3, v_4)$. For each v_i, let the outward normal be $\overrightarrow{n_i}$. For every maximum, we compute the angle $\theta_i = \angle \overrightarrow{n_i}, \overrightarrow{cv_i}$. If $cos(\theta_i) \geq 0$ for all $i = 1 \ldots 4$ and we tag c as `in`, otherwise we mark it `out`.

Clearly, the density of P with respect to Σ plays an important role for this test to succeed. However we note that, by the result of [Chazal and Lieutier 2006; Dey et al. 2005], the critical points of h_P for a well sampled Σ are either near Σ or near the medial axis of Σ. With this test, we are at least able to mark the maxima which lie near the medial axis of Σ and therefore have higher distance function values.

Algorithm: The stable manifold of each maximum is a volumetric subset of $\mathbb{R}^3$ and is approximated by a collection of Delaunay tetrahedra. The stable manifold of the maximum inherits the same `in/out` marking as that of the maximum itself.

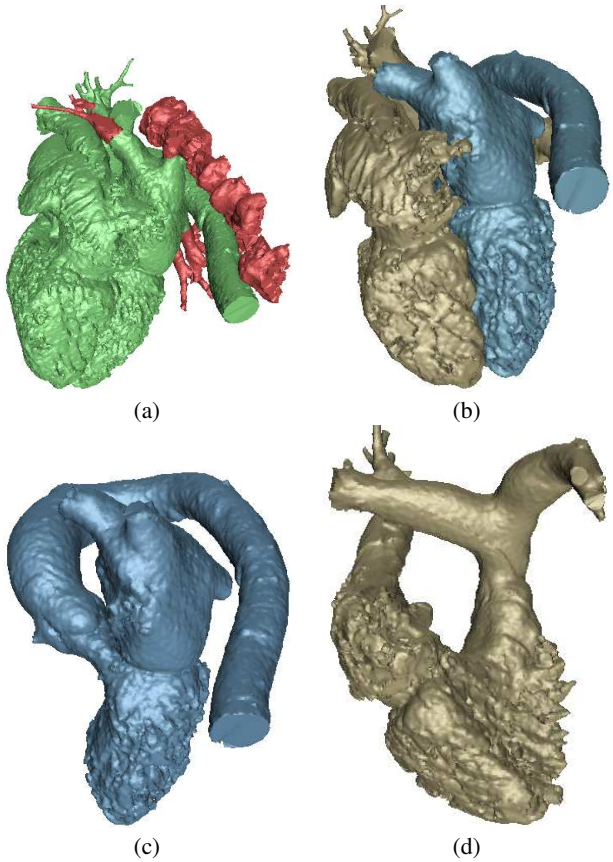

Figure 4: *Results of two-step curation: (a) The resulting clean model of the patient heart (green) along with the extraneous components (red) which are discarded. Note, the left and right subparts are still connected. (b) A stricter merge parameter ($\rho = 5$, described in the text) separates the two subparts as desired. (c,d) The left and right parts are shown separately for visual clarity.*

For curation, we choose only the inner maxima and compute their stable manifolds. The neighboring stable manifolds are then merged carefully. We observe that, when the stable manifolds of two maxima c_1 and c_2 have non-empty intersection and an index-2 saddle s lies at the common intersection, then without loss of generality,

1. if c_1 comes from subvolume which is substantially thinner than the subvolume that c_2 belongs to, then following Fact 2,

$$h_P(c_2) \gg h_P(c_1) \geq h_P(s)$$

, and

2. if both c_1 and c_2 belong to subvolumes which are comparably "fat", but are connected via a thin channel, then following Fact 2,

$$\min\{h_P(c_1), h_P(c_2)\} \gg h_P(s)$$

.

Following the above two relations, we introduce a parameter $\rho \geq 1$ and merge two adjacent stable manifolds, if

$$\min\{\frac{h_P(c_2)}{h_P(s)}, \frac{h_P(c_1)}{h_P(s)}\} \geq \rho$$

Parameter ρ affects how restrictively we merge the subvolumes to form bigger clusters. Bigger the value of ρ, less restrictive it is and therefore it allows the coalescence of stable manifolds with more disparate maxima. We note that similar techniques were also used earlier for free-form object segmentation [Dey et al. 2003] and topological noise removal [Bajaj et al. 2007].

For our purpose, we initially select a high value of ρ, typically around 20 and merge the adjacent stable manifolds to form large clusters hoping that the patient heart will still survive while the thin blood vessels and barely connected bones and tissues will get detached from it. In fact, as is shown in Figure 4, that is indeed the case. The thin vessels and the loosely connected bones and other tissues are collected as union of tetrahedra which are simply removed by changing their in-out tag from `inside` to `outside`. As we further decrease the parameter ρ (around 5), we can separate the left and right part of the patient heart. We must note that ideally they should not have been connected in the first place, because the inner wall of the left and right part are separated by a muscle wall. However in the initial model, they are almost always connected with each other by thin bridges which are merely due to the anomalies present in the imaging data or are contouring artifacts (Figure 3 (d)). The curation process cures such topological inconsistency and produces a clean model of the patient heart which is then used for anatomy-guided annotation.

3.2 Geometry Segmentation

The result of the curation step is a pair of tetrahedral solids which serves as a working geometric model of the patient heart. However, one such geometric model does not carry all the necessary information, as we shall see in the next section. A further semantic description following the true human anatomy is essential to perform the subsequent tasks. Again, one must translate the problem into the geometric domain so that a computational solution can be found. Luckily, the shape of the human heart is such that again the information encoded in the distance function comes to rescue.

Our goal in this step is to decompose the whole patient heart into six main compartments, namely left and right `ventricle`, left and right `atrium`, `aorta` and `pulmonary artery`. We start with two subvolumes, one for the left part and one for the right part of the heart. Each of these sub-parts consists of a ventricle which is roughly ellipsoidal and an atrium and a vessel are connected to it through two relatively narrower disjoint openings. We have already discussed in the last subsection, the pattern of h_P that such geometric model induces. Near the openings, there are index-2 saddles whose stable manifolds form a natural layer and thereby separates the maxima on each side. The stable manifolds of each sub-group of the maxima then describes the ventricle, atrium and aorta or pulmonary artery depending on the left or right side of the heart that we look at.

The task is thus almost similar to the curation step. The user needs to select a suitable value for ρ, which will prevent merging of the stable manifolds of two maxima which are coming from two anatomically different regions. Apparently straight forward, the choosing ρ proves to be quite tricky and in our experience, it is often almost impossible to come up with a single value for ρ that automatically dissects the left or right portion into three desired compartments.

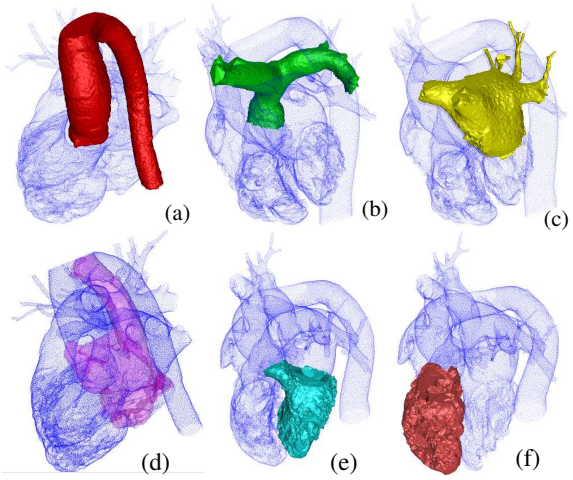

Figure 5: *The segmentation of the patient heart into (a)* `aorta`*, (b)* `pulmonary artery`*, (c)* `left atrium`*, (d)* `right atrium`*, (e)* `left ventricle`*, and (f)* `right ventricle`

To tackle this problem, we add one important utility function that aides in an iterative process by which the user can semi-automatically perform the desired segmentation. Since every stable manifold, and hence the union of two or more of them is essentially a collection of Delaunay tetrahedra, one can easily subtract a certain subset from all the interior Delaunay tetrahedra, and then recursively apply the merging process with different ρ on the rest. Thus the segmentation algorithm works as follows:

- Starting with a Delaunay tetrahedralized volume of either the left or the right portion of the patient heart, we choose a suitable value of ρ which segments one of the desired compartments from the rest. In our experience, typically a value of ρ between 3 and 5 segments the aorta from the left side and the pulmonary artery from the right side.

- Once the segmentation reaches the desired accuracy (measured visually) for one compartment, that component is subtracted from the overall volume and the segmentation with a different ρ is performed on the rest.

Figure 5 shows the performance of the segmentation process on the curated model. The blue cloud around every segmented part shows the whole point set from where the portions are segmented.

4 Construction of Muscle Wall

After the curation and segmentation of the inner wall, we obtain a clean, annotated geometric model of the inner wall. But the modeling process does not stop there as also need to model the muscle wall of the patient heart with proper thickness so that it can support further simulation-based diagnosis and treatment of the mechanical and electrical behavior of the patient heart. This is a relatively well-understood geometric problem. We approach this problem using the concept of *variable* offset surface where each compartment of the inner wall may offer different thickness. This is more realistic because the thickness of the muscle wall is not uniform. For example, left ventricle has to pump oxygenated blood to the whole body through aortic branches and so the muscle thickness around the left ventricle is larger than that around the right ventricle which has to pump blood to the lungs. Moreover, If we consider the possible anomalies present in the patient heart, the problem becomes more involved and asks for a more general solution.

Offset Surface: Modeling by offset surface is well-studied in the area of geometric modeling and manufacturing. Given an orientable surface Σ and one can modify the (unsigned) distance function h_Σ to a *signed* distance function $h_\Sigma^{\pm}$ by multiplying h_Σ with $+1$ (or -1) if the point where the function is evaluated lies `outside` (or `inside`). Now a uniform ε-offset surface, denoted as Σ_ε, is defined as

$$\Sigma_\varepsilon \;=\; \{x | h_\Sigma^{\pm}(x) = \varepsilon\}$$

. Σ_ε, thus defined, is a fixed distance ε away from Σ.

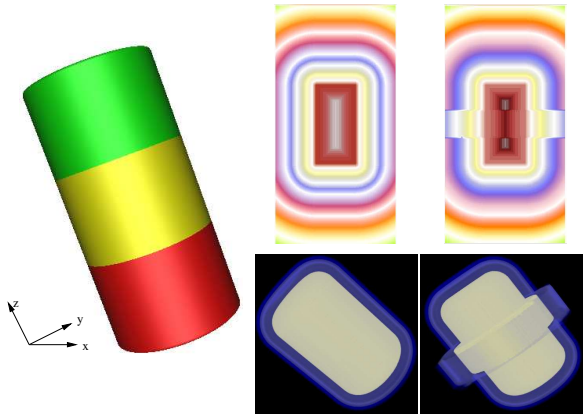

Figure 6: *Left: The test dataset used to explain the generalized distance volume. Middle: Volume rendering of typical distance function using uniform weight on all three parts. Top subfigure shows a single slice on X-Z plane. As the distance function increases, the color changes from yellow to red. Right: Similar result when weights are modified according to the description in the text. Notice, the function is no more continuous and as a result the offset surfaces are not smooth.*

There are numerous prior work that uses and analyzes the properties of offset surface in the context of geometric modeling and manufacturing [Chen and Ravani 1987; Maekawa 1999; Pottmann 1995; Pottmann 1997]. Unfortunately, most of these works consider uniform offsetting around a curve or a surface and therefore does not offer any easy extension to build a muscle wall of variable thickness around different components of the patient heart. Recently, a novel approach to model multi-material volume using distance function was reported in [Biswas et al. 2004]. In this paper, authors presented ways to blend multiple distance function induced by more than one object so that the resulting function can model the density of different materials in the object. However in this way one has to compute a separate distance function for every object which is computationally expensive. Instead of modifying the range of the multi-material distance function we modify the effect of each of the materials in a way that automatically achieves the same effect. Also, we feel the approach presented in this section is more intuitive and within a single object, it can assign different material properties.

Computing Signed Distance Function: Before we proceed further, we would also like to mention that although in Section 3 we have used h_P (or unsigned distance function), we did not really have to compute the function explicitly on any arbitrary point. We only used the connection between h_P and Vor/Del diagram of P and occasionally we have used the function values but only at the critical points where again the circumradius of the dual Delaunay simplex containing that point was the function value.

The extensive use of signed distance function (sdf) in computer graphics, image processing and many other domains makes any further description redundant. However, we want to devote a short paragraph to describe a simple customized algorithm that we implemented for our purpose. In this implementation we take advantage of the fact that the surface Σ is already well-sampled and after the curation and the segmentation steps, it is described as the boundary of a subset of Delaunay tetrahedra from the whole Delaunay triangulation of the points sampling the surface. This essentially means the tetrahedra are marked either `in` or `out`. To determine the sign of any point in $\mathbb{R}^3$, we therefore locate the point within the tetrahedralization and assign the positive or negative sign based on the marking of the tetrahedron. Once the sign is determined, we compute the magnitude of the distance value. Again, since the surface is well-sampled, we first identify the closest vertex on the triangulated boundary using kd-tree. Then we explicitly compute the distance value to every triangle forming the disk-neighborhood around the nearest vertex to get the minimum distance. This substantially improves the time complexity without losing precision much as we see in the results that we present.

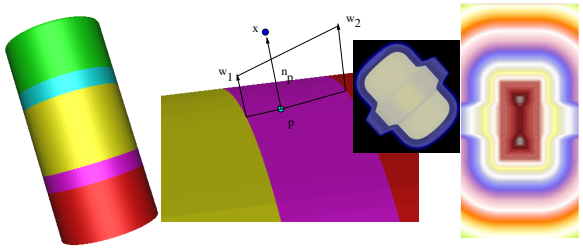

Figure 7: *Smoothing bands are drawn in purple and cyan. For a point x which lies in the smoothing band (purple), the weight is linearly interpolated from the two adjacent materials (with weights w_1 and w_2). Right subfigure shows that the distance volume is continuous and any variable-offset surface is smooth.*

Generalized Offset: The main purpose of building one such generalized distance volume is so that we can select an appropriate isovalue and the isosurface (offset surface) gives a realistic approximation of the muscle wall around the inner wall of the patient heart. Following the segmentation, we assign a scalar weight on the wall of every compartment. Before we talk about the choice of suitable scalar wights, we analyze the effects of these scalar weights on a test dataset.

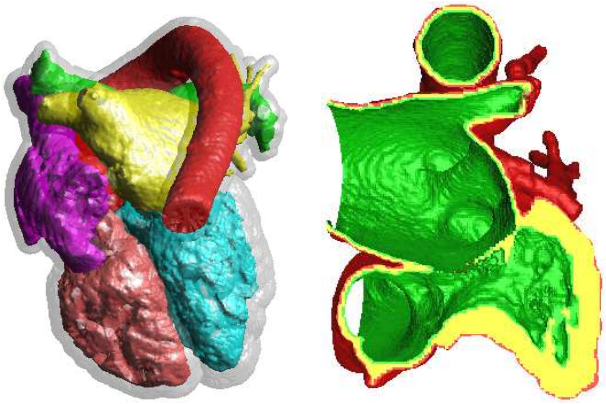

(a) (b)

Figure 8: *(a) Transparent muscle wall around the segmented inner volume. (b) Cut-away of the muscle (yellow) between the inner (green) and outer (red) wall of the left sub-part shows the variable thickness around different components. Notice the thicker muscle around the ventricular region.*

We trisect a capped cylinder and assign three material properties on each part, denoted by three different colors (see Figure 6(a), red - material 1, yellow - material 2, green - material 3). Now we assign equal scalar weights on each part $w_1 = w_2 = w_3 = 1$. The resulting distance volume is just the normal signed distance volume (Figure 6 (middle)). Now we modify the weights $w_1 = 0.5$, $w_2 = 0.3$, $w_3 = 0.5$. The change in the distance function can now be seen in the right subfigure of Figure 6. One can clearly see the difference between the two distance volumes. In particular we see that in the latter case, the distance volume bulges around the yellow sub-part of the inducing object (cylinder in this case). This is not surprising since due to the assignment of a relatively smaller weight in the yellow portion, the distance function grows slower around that region. This is the fundamental idea behind the modeling of variable-thickness muscle wall around the annotated inner wall. But before that, we want to point out some of the undesirable properties of the generalized distance volume and any isosurface that results from that.

Smoothness of Generalized Offset Surface: If one looks at the volume (and slice) rendering of the weighted distance volume, one notices that at the cost of achieving the desired non-uniform thickness, the resulting function is discontinuous and any isosurface (other than the zero-set) will be non-smooth. Not surprisingly, the discontinuity occurs in places where two regions with different weights interfere. So we must cure the problem by changing the weight near the interface of two materials continuously.

To achieve smooth blending of the weights of two different materials, we create a *smoothing band* around the interface in one material and vary the weight of that material so that it matches the weight of the neighboring material at the interface. This process is illustrated in Figure 7, where we have shown two smoothing bands - purple strip within red and cyan strip within green sub-part. The position of the smoothing band is not so important in our application, however ideally one would like it to place it so that it covers both the interfacing regions. We then define an interpolation (linear in Figure 7) and blends the weights within the smoothing band. For any $p \in \mathbb{R}^3$, if the nearest point to the surface (x in Figure 7) falls within any of these bands, we compute the geodesic distance of x from the two interface boundaries on the surface and depending on the interpolation technique used, we assign a new weight at x, say w_x, which we then use to scale the Euclidean distance $\|p-x\|$ and generate the generalized signed distance function value at p. Note, instead of blending the function values in the whole resulting volume which may be quite large and dense, this approach offers additional efficiency as compared to [Biswas et al. 2004].

Variable Thickness of Muscle Wall: Now we are in a position to build a geometric model of the muscle wall that faithfully describe the anatomy. Following the annotation obtained via the segmentation process, we first assign different weights on the surfaces of the aorta, left ventricle and so on. As mentioned earlier, the muscle thickness around left and right ventricle are more than any other part, and so we assign the smallest weight to left ventricle and the second smallest weight to the right ventricle. We then compute the generalized distance volume as described and select a suitable isovalue to output the geometric model of the muscle wall of the whole heart. Figure 8 shows the muscle wall around the segmented inner volume. We have implemented the algorithm of [Labelle and Shewchuk 2007] to produce the tetrahedral mesh of the muscle wall. The variation of thickness around different sub-parts is clearly seen.

5 Implementation and Results

5.1 Implementation

All three steps discussed in this paper heavily rely on a robust implementation of Voronoi/Delaunay diagram of a set of point in three dimension. We have used CGAL to construct these two datastructures as it offers numerical robustness and handles nearly degenerate cases gracefully [CGAL Consortium 2007]. However CGAL only provides the base classes for these structures which we have inherited and enhanced according to our own needs. Other than construction of the Voronoi/Delaunay datastructure, we have also used the point location algorithm in CGAL to assign the sign of the signed distance function value.

For volume rendering of the distance volume and the input imaging data, we have used the open source volume visualization software VolRover [CVC, UT Austin 2005] and for the rendering of the geometric models we have used geomview [Geometry Center, University of Minnesota 1996].

5.2 Timing

In this paper we have described three key steps of the geometry processing sub-unit of our IMAGING-MODELING framework. In this subsection, we briefly mention the complexity of each step and the time it took in each step to build the final model. All the computations were done on a machine with quad 2.4 GHz AMD Opteron processors and 8GB RAM. The codes were compiled using `g++` (*version 4.1.1*) with optimization flag -O1.

The curation and segmentation steps both work on the Delaunay triangulation of the point set sampling the surface at any stage. Computing the triangulation of a point set of size 351K took 80 seconds. Tagging the tetrahedra `in` and `out` and subsequently computing the stable manifolds took only 15 seconds. The curation and segmentation steps then require possibly repetitive merging of the stable manifolds with different merge parameters (ρ) and each such merge takes only a few (less than 2) seconds.

The generalized offsetting step builds a distance volume and samples it on a three dimensional volume of resolution $257 \times 257 \times 257$ grid. With the modified distance computation (described in Section 4), this step took only about 2 minutes. The last step is to compute the tetrahedral mesh of the muscle wall which took about 1 minute.

5.3 Results

We tested our algorithm on a patient CT scan provided by Dr. Charlie Walvaert of Austin Heart Hospital, USA. The original CT image is of dimension $512 \times 512 \times 368$ and the spacing in x, y, z directions are respectively 0.439 *mm*, 0.439 *mm*, 0.5 *mm*. Figure 9 shows the performance of our algorithm on this sample dataset. We have used the following parameters to construct the muscle wall shown in Figure 9. The weights to construct generalized offset volume are as follows - weights of Atria, Aorta and Pulmonary Artery are unity; of right ventricle it is 0.75; of left ventricle it is 0.5. The outer boundary of the muscle wall is then described as the isocontour corresponding to isovalue 0.74 and the solid mesh is created as an interval volume between two contours corresponding to 0 and 0.74 using the algorithm of [Labelle and Shewchuk 2007]. The choice of the value is arbitrary and the modeling algorithm accommodates any scalar value. However this particular choice should be guided by an expert. We are currently examining certain topological invariants that the muscle wall should possess which should automatically guide the choice of the parameters to produce the interval volume (and hence the solid muscle wall) that is anatomically correct.

6 Conclusions

In this paper, we have described three main steps of a comprehensive framework to construct a suitably discretized, anatomically correct, patient-specific geometric model of human heart from real CT imaging data. We have explained the challenges that often arise with such imaging data and have shown evidences how robustly and effectively these algorithms perform. A suitable (generalized) distance function is the key ingredient of all three algorithms. We are currently exploring ways to interactively manipulating the distance volume to give real-time feedback to the user so that one can more efficiently build a geometric model following the patient parameters.

Acknowledgement: This research was supported in part by NSF grant CNS-0540033 and NIH contracts P20-RR020647, R01-EB00487, R01-GM074258, R01-GM07308. We thank Dr. Charlie Walvaert of the Austin Heart Hospital, USA for providing the CT64 thoracic scan. Thanks are also due to Joe Rivera of Computational Visualization Center at UT Austin for his immense help with data processing. Finally, we thank the anonymous reviewers for their helpful comments that helped improve this manuscript.

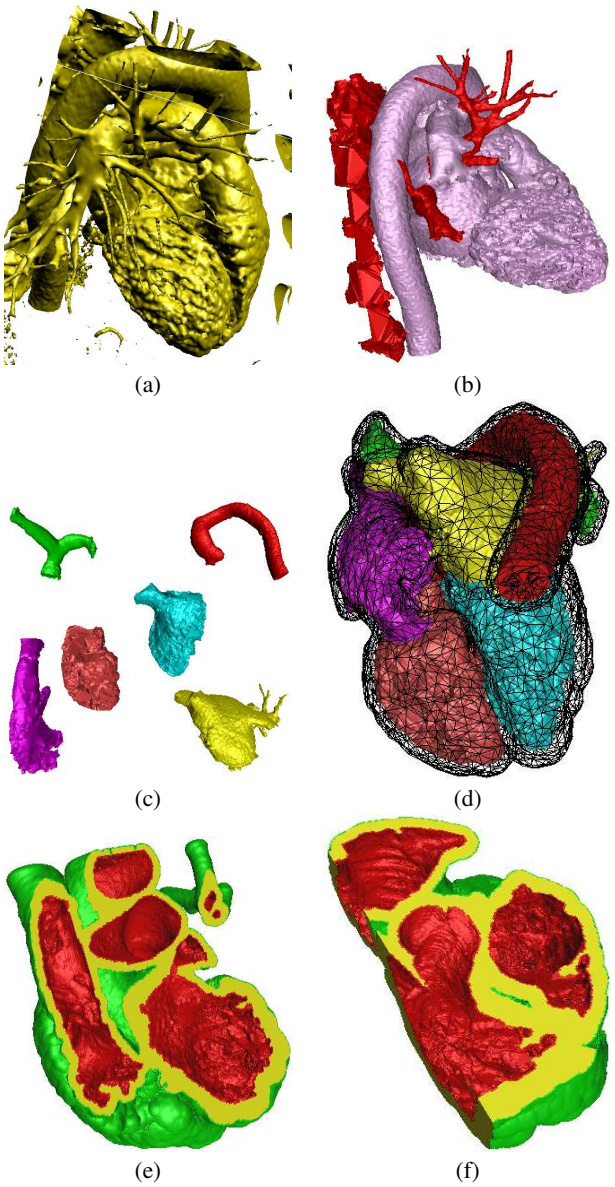

Figure 9: *(a) Initial Model extracted from the imaging data. (b) Curated model with the spurious components colored red (and subsequently discarded). (c) Segmented parts of the inner wall are shown in a scattered position. (d) Wire-frame rendering of the variable-width muscle wall around the segmented inner wall. (e, f) Two cuts of the tetrahedral volumetric mesh to emphasize the different width of the muscle around different components.*

References

ALLOUCHE, C. F., MAKAM, S., AYACHE, N., AND DELINGETTE, H. 2001. A new kinetic modeling scheme for the human left ventricle wall motion with mr-tagging imaging. In *Functional Imaging and Modeling of Heart*, T. Katila, I. E. Magnin, P. Clarysse, J. Montagnat, and J. Nenonen, Eds., LNCS, 61–68.

BAJAJ, C., AND GOSWAMI, S. 2006. Automatic fold and structural motif elucidation from 3d em maps of macromolecules. In *ICVGIP 2006*, 264–275.

BAJAJ, C., AND XU, G. 2001. Smooth shell construction with mixed prism fat surfaces. *Brunett, G., Bieri,H., Farin, G. (eds.), Geometric Modeling Computing Supplement 14*, 19–35.

BAJAJ, C., AND XU, G. 2003. Anisotropic diffusion of surfaces and functions on surfaces. *ACM Transactions on Graphics 22*, 1, 4–32.

BAJAJ, C., GOSWAMI, S., YU, Z., ZHANG, Y., BAZILEVS, Y.,

AND HUGHES, T. 2006. Patient specific heart models from high resolution ct. In *Proceedings of Computational Modelling of Objects Represented in Images, CompIMAGE*, 157–165.

BAJAJ, C., GILLETTE, A., AND GOSWAMI, S. 2007. Topology based selection and curation of level sets. In *Topology-in-Visualization*, A. Wiebel, H. Hege, K. Polthier, and G. Scheuermann, Eds.

BISWAS, A., SHAPIRO, V., AND TSUKANOV, I. 2004. Heterogeneous material modeling with distance fields. *Computer Aided Geometric Design 21*, 3, 215–242.

BRAESS, D. 1995. Towards algebraic multigrid for elliptic problems of second order. *Computing 55*, 379–393.

BROWN, P., BYRNE, G., AND HINDMARSH, A. 1989. VODE: A variable-coefficient ode solver. *SIAM Journal on Scientific Computation 10*, 1038–1057.

CGAL CONSORTIUM. 2007. CGAL (3.3.1): Computational Geometry Algorithms Library. *http://www.cgal.org*.

CHAZAL, F., AND LIEUTIER, A. 2004. Stability and homotopy of a subset of the medial axis. In *Proc. 9th ACM Sympos. Solid Modeling and Applications*, 243–248.

CHAZAL, F., AND LIEUTIER, A. 2006. Topology guaranteeing manifold reconstruction using distance function to noisy data. In *Sympos. on Comput. Geom.*, 112–118.

CHEN, Y. J., AND RAVANI, B. 1987. Offset surface generation and contouring in computer-aided design. *Journal of Mech. Trans. Autom. Design 109*, 1, 133–142.

COSTA, K. D., HUNTER, P. J., WAYNE, J. S., WALDMANN, L. K., GUCCIONE, J. M., AND MCCULLOCH, A. D. 1996. A three-dimensional finite element method for large elastic deformations of ventricular myocardium: Ii - prolate spheroidal coordinates. *J. Biomedical Engineering 118*, 4 (November), 464–472.

CVC, UT AUSTIN. 2005. Volrover. *http://cvcweb.ices.utexas.edu/software/guides.php*.

DE MUNCK, J. 1992. A linear discretization of the volume conductor boundary integral equation using analytically integrated elements. *IEEE Trans Biomed. Eng. 39*, 9 (September), 986–990.

DEY, T. K., AND GOSWAMI, S. 2003. Tight cocone: A water-tight surface reconstructor. In *Proc. 8th ACM Sympos. Solid Modeling and Applications*, 127–134.

DEY, T. K., AND GOSWAMI, S. 2004. Provable surface reconstruction from noisy samples. In *Proc. 20th ACM-SIAM Sympos. Comput. Geom.*, 330–339.

DEY, T. K., GIESEN, J., AND GOSWAMI, S. 2003. Shape segmentation and matching with flow discretization. In *Proc. Workshop Algorithms Data Strucutres (WADS 03)*, F. Dehne, J.-R. Sack, and M. Smid, Eds., LNCS 2748, 25–36.

DEY, T. K., GIESEN, J., RAMOS, E., AND SADRI, B. 2005. Critical points of the distance to an epsilon-sampling of a surface and flow-complex-based surface reconstruction. In *Proc. 21st ACM-SIAM Sympos. Comput. Geom.*, 218–227.

EDELSBRUNNER, H., FACELLO, M. A., AND LIANG, J. 1998. On the definition and the construction of pockets in macromolecules. *Discrete Apl. Math. 88*, 83–102.

EDELSBRUNNER, H. 2002. Surface reconstruction by wrapping finite point sets in space. In *Ricky Pollack and Eli Goodman Festschrift*, B. Aronov, S. Basu, J. Pach, and M. Sharir, Eds. Springer-Verlag, 379–404.

GEOMETRY CENTER, UNIVERSITY OF MINNESOTA. 1996. Geomview. *http://www.geomview.org/*.

GIESEN, J., AND JOHN, M. 2003. The flow complex: a data structure for geometric modeling. In *Proc. 14th ACM-SIAM Sympos. Discrete Algorithms*, 285–294.

GOERRES, G. W., KAMEL, E., SEIFERT, B., BURGER, C., BUCK, A., HANY, T. F., AND SCHULTHESS, G. K. V. 2002. Accuracy of image coregistration of pulmonary lesions in patients with non-small cell lung cancer using an integrated pet/ct system. *Journal Nucl. Med. 43*, 1469–1475.

GOSWAMI, S., DEY, T. K., AND BAJAJ, C. L. 2006. Identifying flat and tubular regions of a shape by unstable manifolds. In *Proc. 11th Sympos. Solid and Physical Modeling*, 27–37.

GOSWAMI, S., GILLETTE, A., AND BAJAJ, C. 2007. Efficient Delaunay mesh generation from sampled scalar function. In *Proc. 16th Int. Meshing Roundtable*, 495–511.

HACKBUSCH, W. 1985. *Multi-Grid Methods and Applications*. Springer Verlag, Berlin, Heidelberg, New York, Tokyo.

HILLE, B. 1992. *Ionic Channels of Excitable Membranes.*, Second ed. Sinauer Associates, Inc., Sunderland, MA.

HODGKIN, A. L., AND HUXLEY, A. F. 1952. A quantitative description of membrane current and its application to conduction and excitation in nerve. *Journal of Physiology 117*, 500–544.

HUNTER, P., MCCULLOCH, A., NIELSEN, P., AND SMAILL, B. 1988. A finite element model of passive ventricular mechanics. *ASMS BED 9*, 387–397.

JU, T., LOSASSO, F., SCHAEFER, S., AND WARREN, J. 2002. Dual contouring of hermite data. In *SIGGRAPH 2002, Computer Graphics Proceedings*, ACM Press / ACM SIGGRAPH, 339–346.

LABELLE, F., AND SHEWCHUK, J. R. 2007. Isosurface stuffing: fast tetrahedral meshes with good dihedral angles. *ACM Transactions on Graphics 26*, 3.

LORENSEN, W., AND CLINE, H. 1987. Marching Cubes: A High Resolution 3D Surface Construction Algorithm. In *SIGGRAPH*, 163–169.

LUO, C., AND RUDY, Y. 1991. A model of the ventricular cardiac action potential: Depolarization, repolarization and their interaction. *Circulation Research 68*, 6, 1501–1526.

LUO, C., AND RUDY, Y. 1994. A dynamic model of the cardiac ventricular action potential: I. simulations of ionic currents and concentration changes. *Circulation Research 74*, 6, 1071–1096.

MAEKAWA, T. 1999. An overview of offset curves and surfaces. *Computer-Aided Design 31*, 3, 165–173.

MARI, J.-L., ASTART, L., AND SEQUEIRA, J. 2001. Geometrical modeling of the heart and its main vessels. In *Functional Imaging and Modeling of Heart*, T. Katila, I. E. Magnin, P. Clarysse, J. Montagnat, and J. Nenonen, Eds., LNCS, 10–16.

MCVEIGH, E., FARIS, O., ENNIS, D., HELM, P., AND EVANS, F. 2001. Measurement of ventricular wall motion, epicardial electrical mapping, and myocardial fiber angles in the same heart. In *Functional Imaging and Modeling of Heart*, T. Katila, I. E.

Magnin, P. Clarysse, J. Montagnat, and J. Nenonen, Eds., LNCS, 76–82.

MULLER, C., ROMBAUT, M., AND JANIER, M. 2001. Dempster shafer approach for high level data fusion applied to the assessment of myocardial viability. In *Functional Imaging and Modeling of Heart*, T. Katila, I. E. Magnin, P. Clarysse, J. Montagnat, and J. Nenonen, Eds., LNCS, 104–112.

PINSKY, H., DYDA, S., PINSKY, R., MISCH, K., AND SARMENT, D. 2006. Accuracy of three-dimensional measurements using cone-beam ct. *Dentomaxillofac. Radiol. 35*, 6, 410–416.

POTTMANN, H. 1995. Rational curves and surfaces with rational offsets. *Computer Aided Geometric Design 12*, 2, 175–192.

POTTMANN, H. 1997. General offset surfaces. *Neural, Parallel & Scientific Computationsi 5*, 1-2, 55–80.

ROGERS, J. M., AND MCCULLOCH, A. D. 1994. A collocation-galerkin finite element model of cardiac action potential propagation. *IEEE Trans Biomed. Eng. 41*, 743–757.

RUDY, Y., AND PLONSEY, R. 1980. A comparison of volume conductor and source geometry effects on body surface and epicardial potentials. *Circ. Res. 46*, 283–291.

SACHSE, F. B. 2004. *Computational Cardiology: Modeling of Anatomy, Electrophysiology, and Mechanics.* LNCS 2966. Springer, Berlin, Heidelberg, New York.

SAHNI, O., MUELLER, J., JANSEN, K. E., SHEPHARD, M. S., AND TAYLOR, C. A. 2005. Efficient anisotropic adaptive discretization of the cardiovascular system. Tech. rep., RPI.

SAHNI, O. 2005. *Adaptive procedure for efficient blood-flow simulations*. PhD thesis, RPI.

SIERSMA, D. 1999. Voronoi diagrams and morse theory of the distance function. In *Geometry in Present Day Science*, O. E. Barndorff and E. B. V. Jensen, Eds. 187–208.

SIMELIUS, K., NENONEN, J., AND HORACEK, B. M. 2001. Simulation of anisotropic propagation in the myocardium with a hybrid bidomain model. In *Functional Imaging and Modeling of Heart*, T. Katila, I. E. Magnin, P. Clarysse, J. Montagnat, and J. Nenonen, Eds., LNCS, 140–147.

TAYLOR, C., HUGHES, T., AND ZARINS, C. 1998. Finite element modeling of 3-dimensional pulsatile flow in the abdominal aorta: Relevance to atherosclerosis. *Annals of Biomedical Engineering 26*, 6, 1–13.

TAYLOR, C., HUGHES, T., AND ZARINS, C. 1998. Finite element modeling of blood flow in arteries. *Computer Methods in Applied Mechanics and Engineering 158*, 1-2, 155–196.

TAYLOR, C., HUGHES, T., AND ZARINS, C. 1999. Effect of exercise on hemodynamic conditions in the abdominal aorta. *Journal of Vascular Surgery 29*, 1077–89.

TILG, B., MODRE, R., FISCHER, G., HANSER, F., MESSNARZ, B., AND ROITHINGER, F. X. 2001. Imaging of electrical function within the human atrium and ventricle from paced ecg mapping data. In *Functional Imaging and Modeling of Heart*, T. Katila, I. E. Magnin, P. Clarysse, J. Montagnat, and J. Nenonen, Eds., LNCS, 148–156.

TOSHIBA MEDICAL SYSTEMS - 64 SLICE CT. 2006. Clinical advancement in volumetric CT.

VEISTERA, H., AND LOTJONEN, J. 2001. Reconstructing 3d boundary element heart models from 2d biplane fluoroscopy. In *Functional Imaging and Modeling of Heart*, T. Katila, I. E. Magnin, P. Clarysse, J. Montagnat, and J. Nenonen, Eds., LNCS, 17–23.

VETTER, F., MCCULLOCH, A., AND ROGERS, J. 1998. A finite element model of passive mechanics and electrical propagation in the rabbit ventricles. *Computers in Cardiology*, 705–708.

WINSLOW, R. L., SCOLLAN, D. F., HOLMES, A., YUNG, C. K., ZHANG, J., AND JAFRI, M. S. 2000. Electrophysiological modeling of cardiac ventricular function: From cell to organ. *Annual Reviews in Biomedical Engineering 2*, 119–155.

YIN, L., LUO, X., AND SHEPHARD, M. S. 2005. Identifying and meshing thin sections of 3-d curved domains. Tech. rep., RPI.

YU, Z., AND BAJAJ, C. 2002. Normalized gradient vector diffusion and image segmentation. In *Proceedings of European Conference on Computer Vision*, 517–530.

YU, Z., AND BAJAJ, C. 2004. A fast and adaptive algorithm for image contrast enhancement. In *Proc of IEEE International Conference on Image Processing*, 1001–1004.

ZHANG, Y., , BAJAJ, C. L., AND XU, G. 2008. Surface smoothing and quality improvement of quadrilateral/hexahedral meshes with geometric flow. *Communications in Numerical Methods in Engineering*, To appear .